極低温から常温域での熱物性測定あれこれ

富山大学大学院　理工学研究部(工学)　　平澤　良男

熱拡散率, 比熱, 熱伝導率, 潜熱,
吸着特性, ふく射性質?

充てん層, 粉体, 焼結体, 吸着剤, 吸着質?

定常法, 非定常法(細線加熱法, レーザーフラッシュ法), DSC測定 etc

極低温での熱伝導率測定装置と有効熱伝導率推算モデル

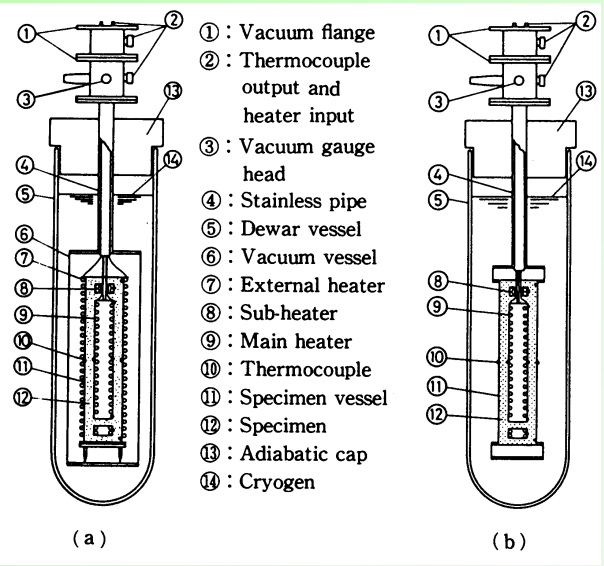

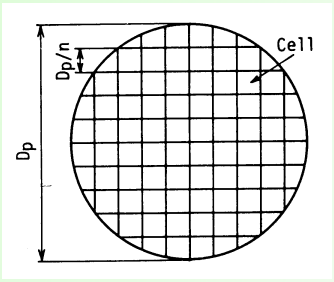

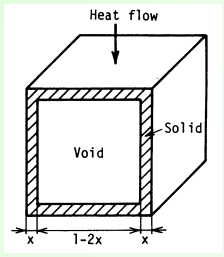

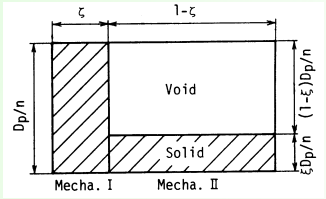

表 1　粒子およびガスの熱伝導率（圧力：1気圧）

温度 t °C	熱伝導率 λ_s, λ_g kcal/mh°C			
	−150	−100	−50	0
ガラス	0.58	0.71	0.82	0.91
青銅	21	27	33	39
銅	246	283	311	317
ステンレス	8.2	9.4	10.3	11.2
窒素	0.0098	0.0137	0.0173	0.0207

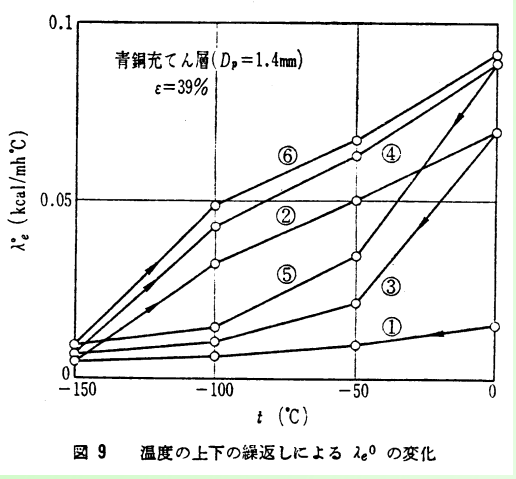

図 9　温度の上下の繰返しによる λ_e^0 の変化

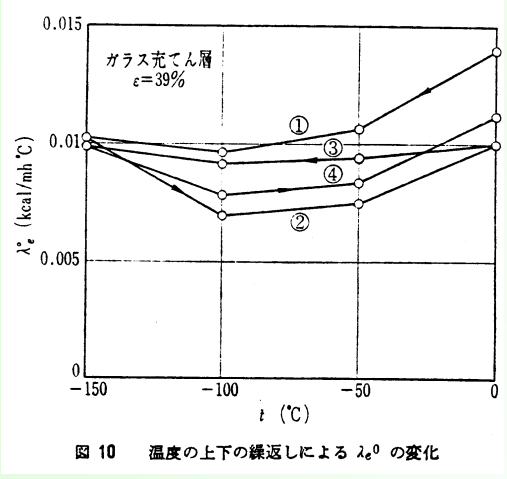

図 10　温度の上下の繰返しによる λ_e^0 の変化

Specimen	Grain size of particle mm	Density of particle kg/m³	Density of powder ρ kg/m³
Perlite B	2.5 - 0.15	-	119
〃 C	〃	-	185
〃 D	1.2 - 0.15	-	87
〃 E	〃	-	71
〃 F	〃	-	63
〃 C_2	1.4 - 1.0	-	146
Glass bubbles			
B37	0.13-0.02	340 - 400	210
B15	〃	120 - 180	80

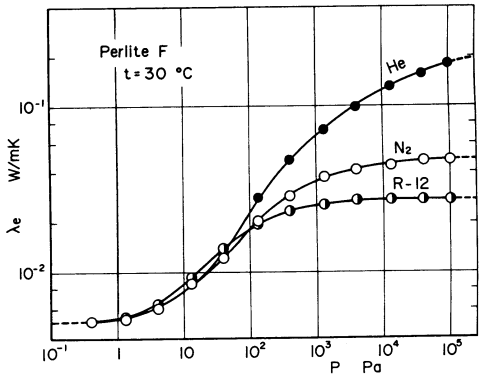

図 5　有効熱伝導率とガス圧力の関係

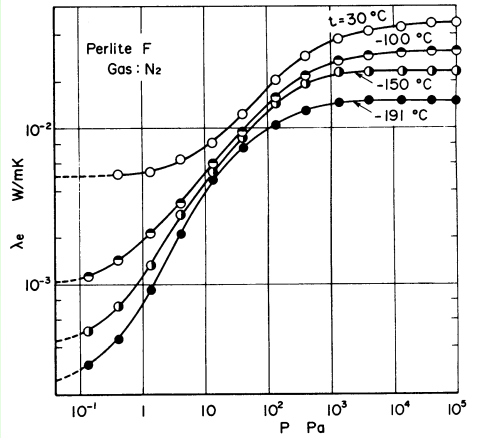

図 6　有効熱伝導率とガス圧力の関係

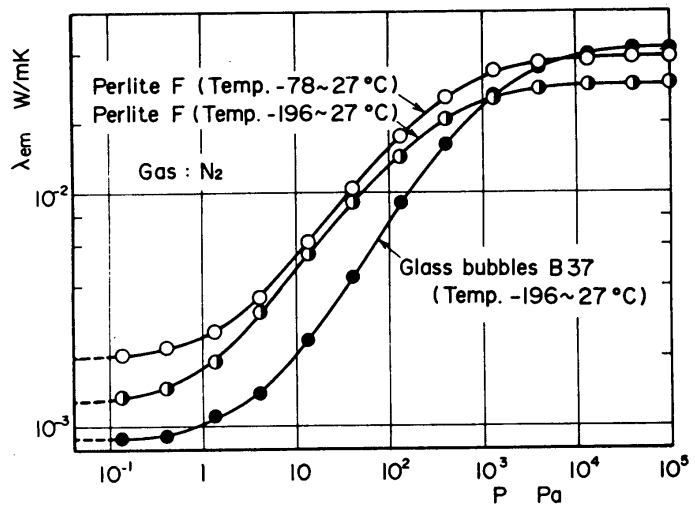

図 10　粉体の温度差の大きい場合の平均有効熱伝導率とガス圧力の関係

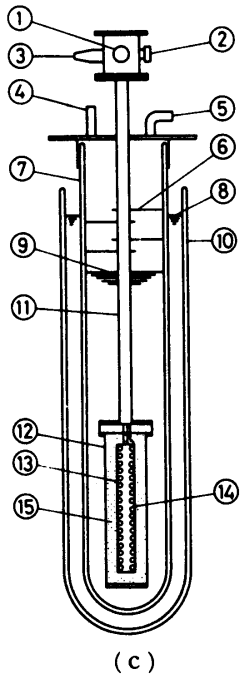

(c)

① Vacuum gauge head
② Thermocouple output and heater input
③ To vacuum
④ Liquefied helium inlet
⑤ Helium gas outlet
⑥ Radiation shield plate
⑦ Inner dewar vessel
⑧ Liquefied nitrogen
⑨ Liquefied helium
⑩ Outer dewar vessel
⑪ Stainless pipe
⑫ Specimen vessel
⑬ Main heater
⑭ Thermocouple
⑮ Specimen

図 1　極低温実験装置の概略

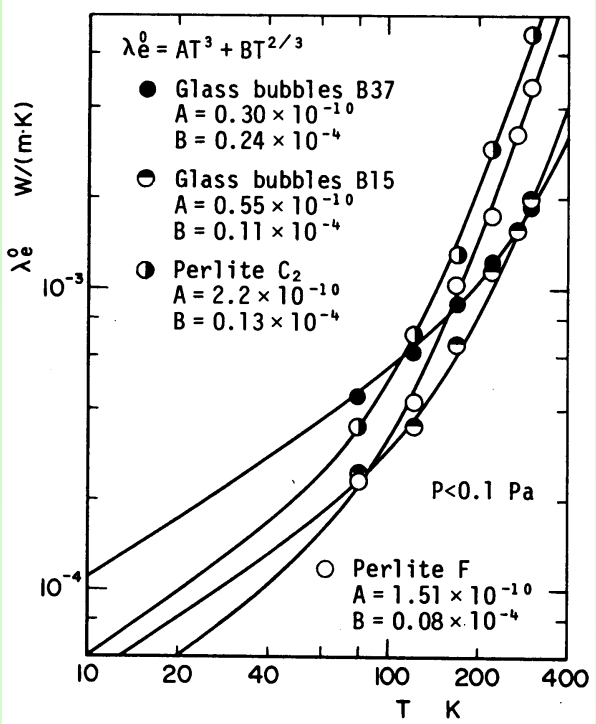

図 2　有効熱伝導率と温度の関係

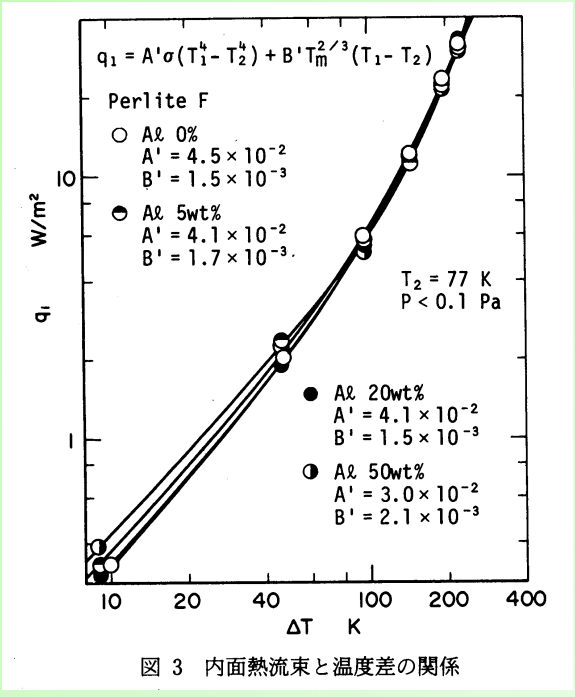

図 3　内面熱流束と温度差の関係

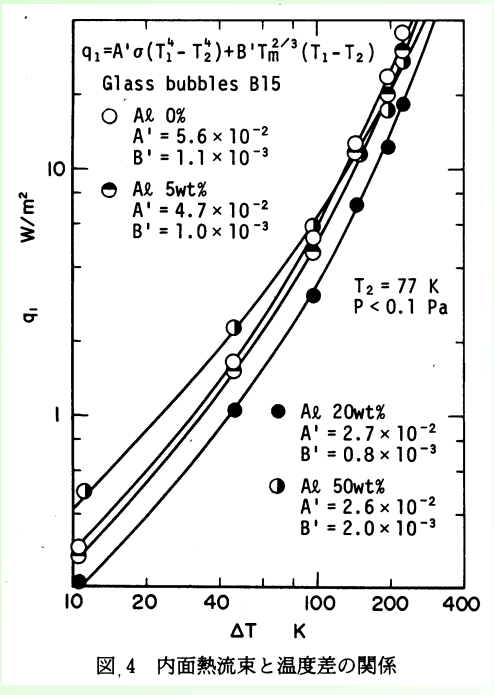

図 4　内面熱流束と温度差の関係

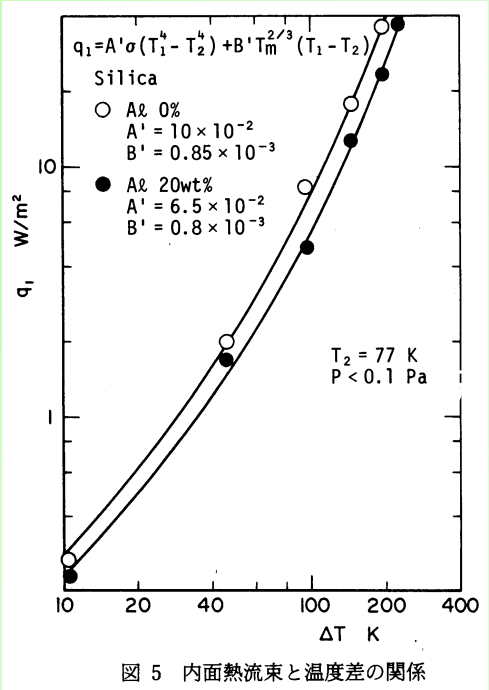

図 5　内面熱流束と温度差の関係

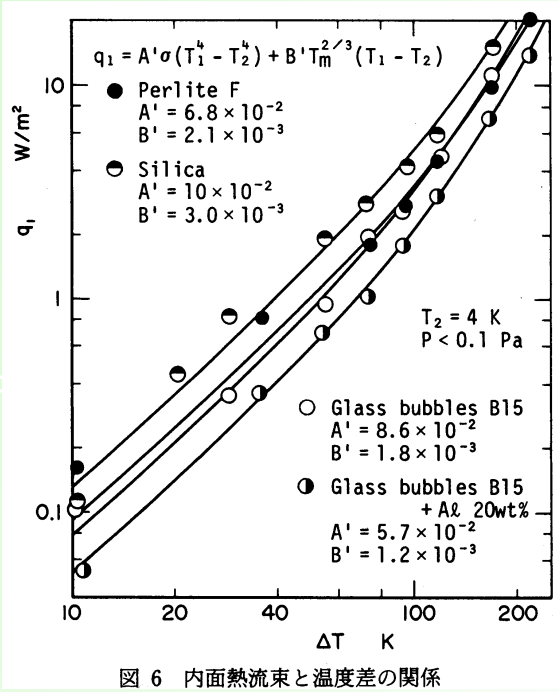

図 6　内面熱流束と温度差の関係

表 3　全熱流束に対するふく射寄与の割合

Specimen	ΔT K / T_2 K	Radiation contribution %			
		10	73	150	223
Perlite F	77	17	32	51	65
	4	0.16	7.0	27	48
Glass bubbles B15	77	25	44	64	76
	4	0.24	9.9	36	58
Glass bubbles B15 + Aℓ20wt%	77	18	34	54	68
	4	0.24	9.9	35	57
Silica	77	44	65	80	88
	4	0.17	7.2	28	49

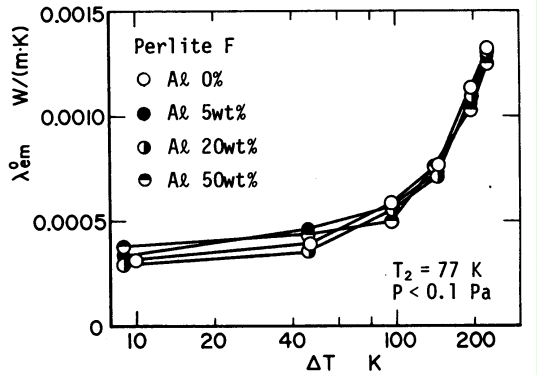

図 7　平均有効熱伝導率と温度差の関係

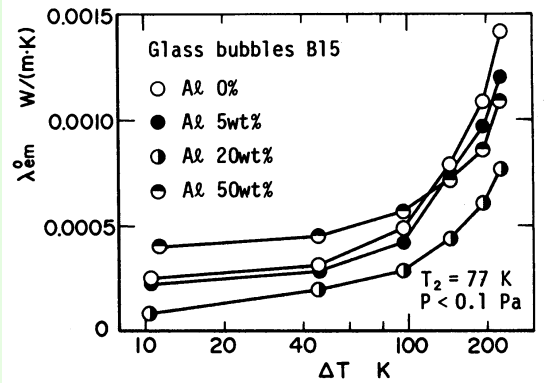

図 8　平均有効熱伝導率と温度差の関係

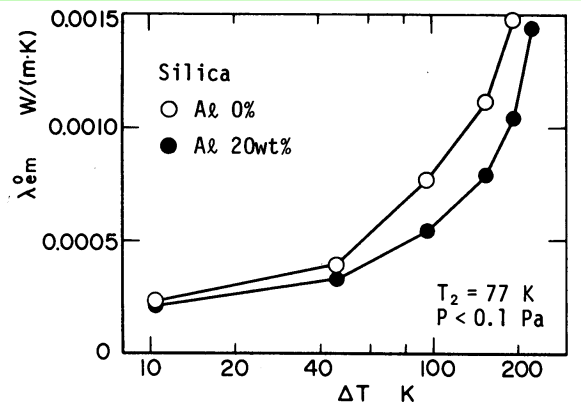

図 9　平均有効熱伝導率と温度差の関係

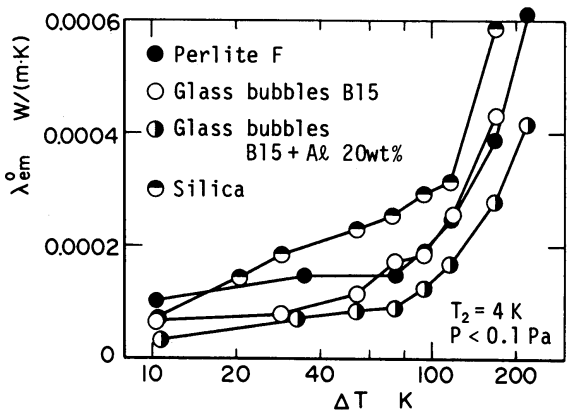

図 10　平均有効熱伝導率と温度差の関係

二元系酸化物の熱定数測定

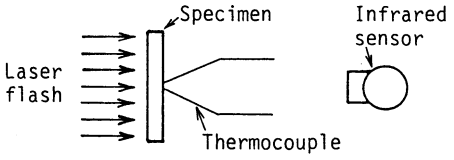

Fig. 1 Principle of laser flash method

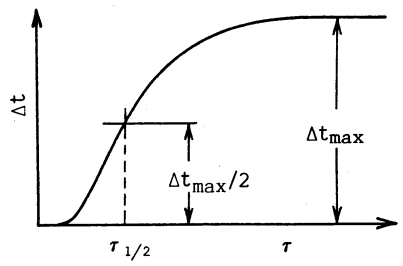

Specimen	Composition ratio Nd_2O_3 : CeO_2 : CuO		Sintering condition O_2 (v%)	Bulk density (g/cm³)
	Mol ratio	Weight ratio		
N1	1 : 0 : 1	4.23 : 0 : 1	0.78	6.14
N2	1 : 0 : 1	4.23 : 0 : 1	21.0	6.55
N3	1 : 0 : 1	4.23 : 0 : 1	64.0	6.73
N4	1 : 0 : 1	4.23 : 0 : 1	100	6.73
N5	0.91: 0.18 :1	3.85 :0.39 :1	21.0	6.87

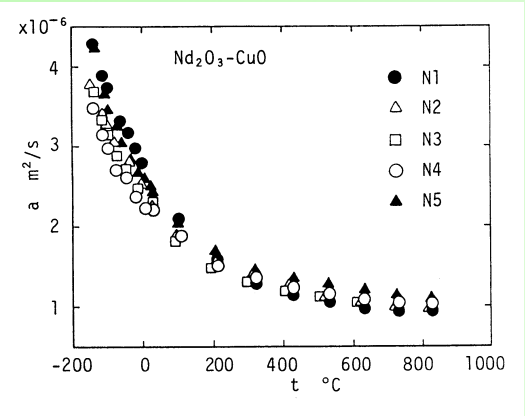

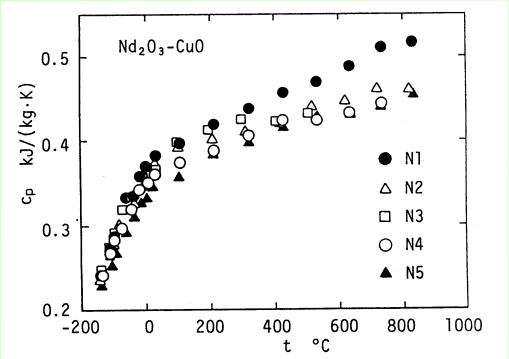

Fig. 9 Specific heat of Nd_2O_3-CuO

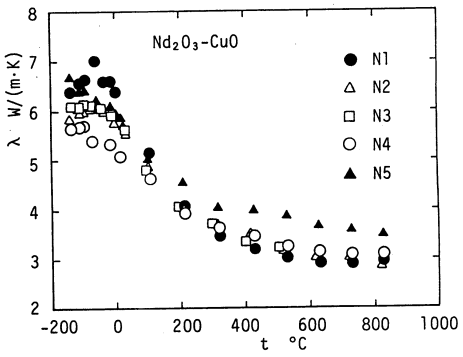

Fig. 10 Thermal conductivity of Nd_2O_3-CuO

吸着剤に含まれる水（氷）の熱物性

Table 1 Physical properties of Silica gel

Specimen	Pore size nm	Maximum ratio of adsorbed water	Density kg/m^3	Specific Surface area m^2/g	Total adsorption heat, J/g
Silica gel					
MB-3A	2.5	0.4	2.66 x10^3	650 x10^3	168
MB-4B	7.0	1.2	2.66	650	158
MB-5D	10.0	1.2	2.66	280	41
MB-300	30.0	1.1	2.66	100	-
MB-500	50.0	1.2	2.66	80	-
MB-800	80.0	1.1	2.66	50	-
MB-1000	100.0	1.3	2.66	30	-
Zeolite					
A-3	0.3	0.2	2.72	783	1100
A-4	0.4	0.2	2.55	726	1018
F-9	0.9	0.26	2.69	721	1082

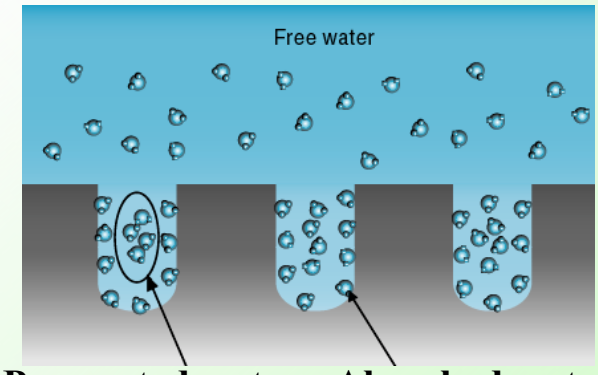

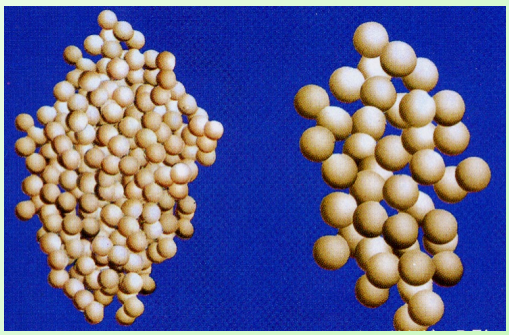

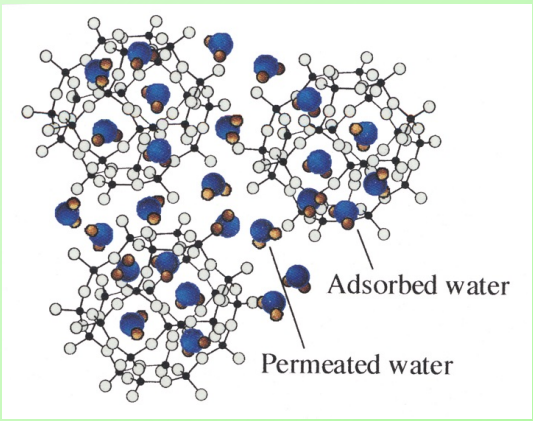

示差走査熱量測定装置（DSC）

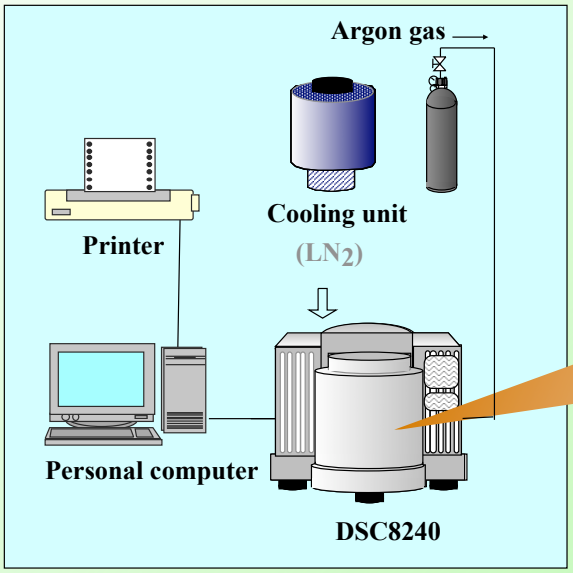

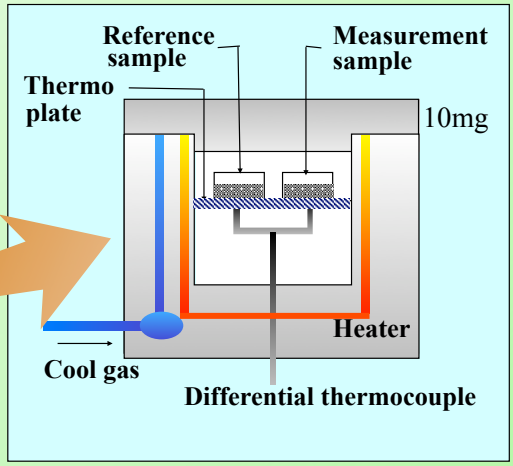

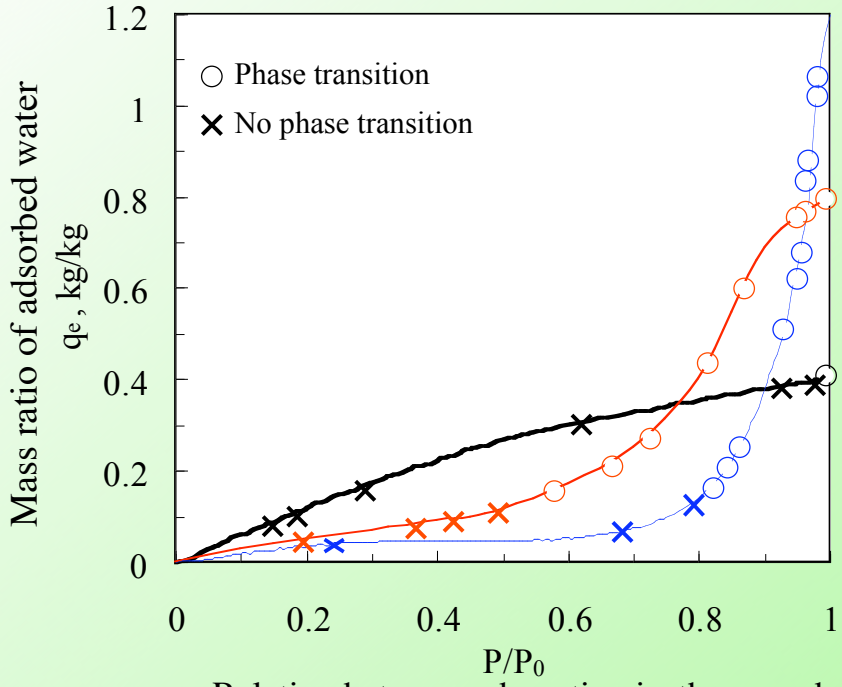

Relation between adsorption isotherm and phase change of water

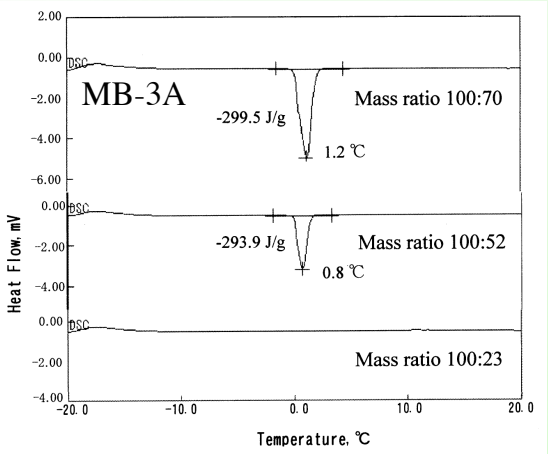

DSC curve for Silica gel MB-3A including water

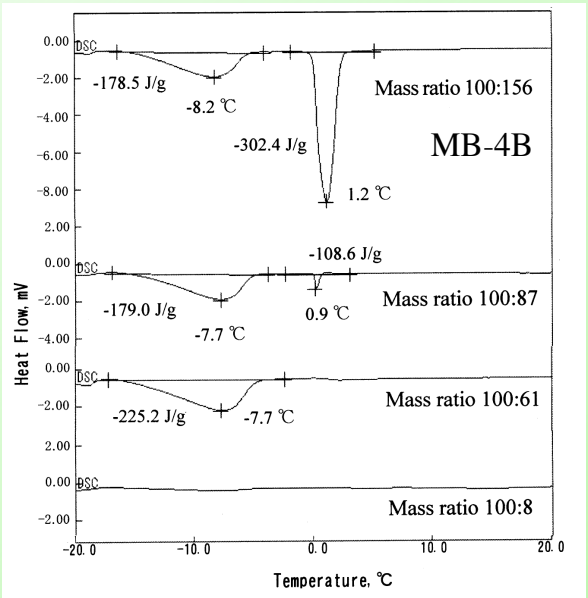

DSC curve for Silica gel MB-4B including water

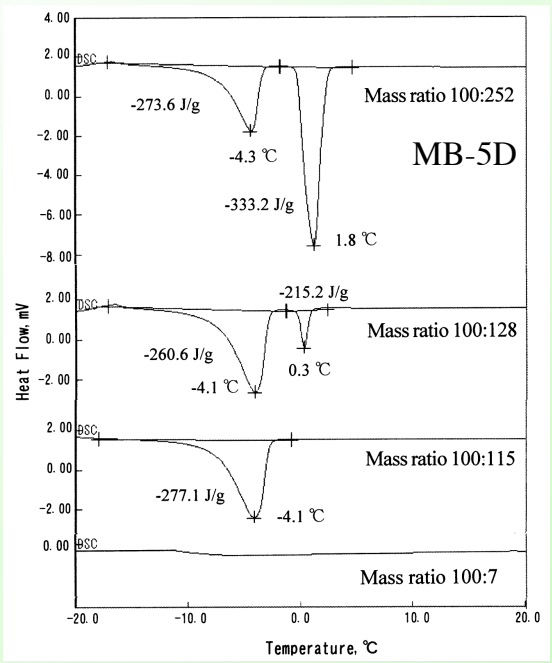

DSC curve for Silica gel MB-5D including water

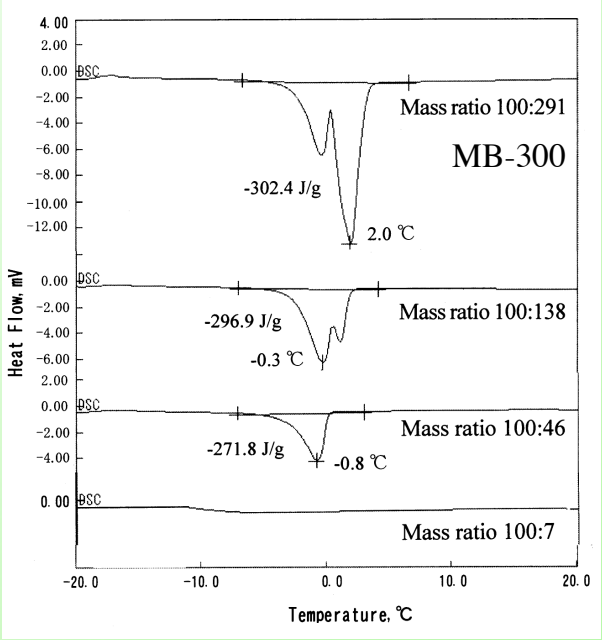

DSC curve for Silica gel MB-300 including water

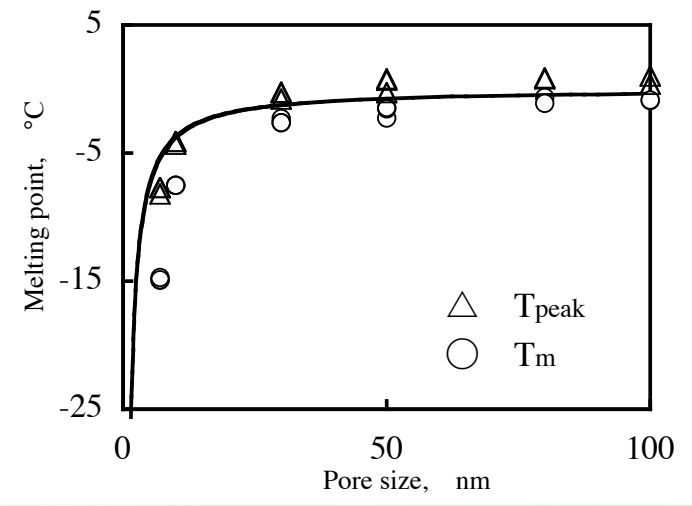

Relationship between melting point of ice and pore size

水分を含有した吸着剤の有効熱伝導率

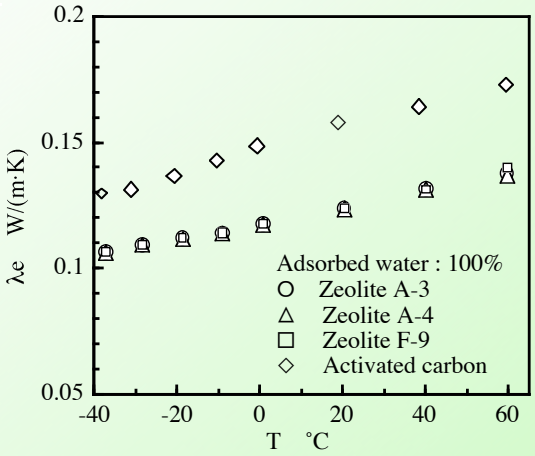

Fig.6 Relation between effective thermal conductivity of packed bed of each particle and temperature

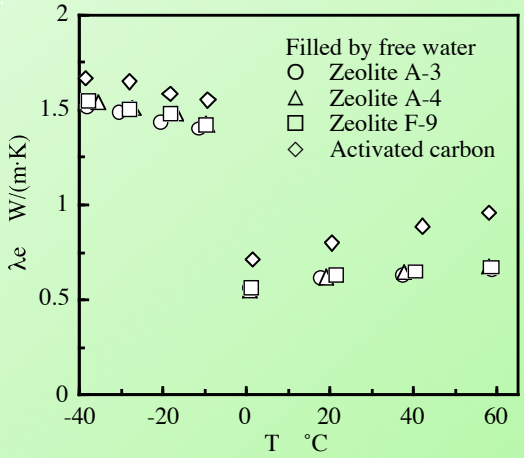

Fig.8 Relation between effective thermal conductivity of packed bed of each particle filled by free water and temperature

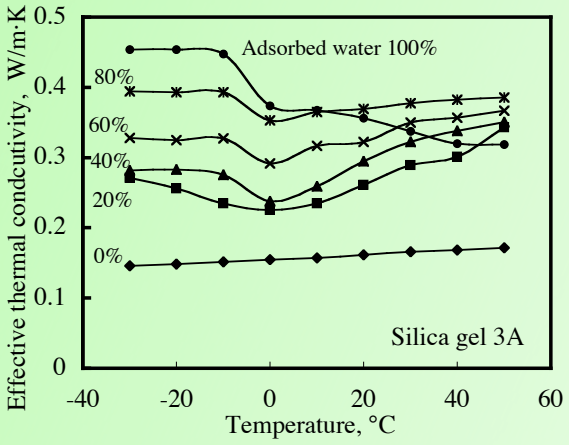

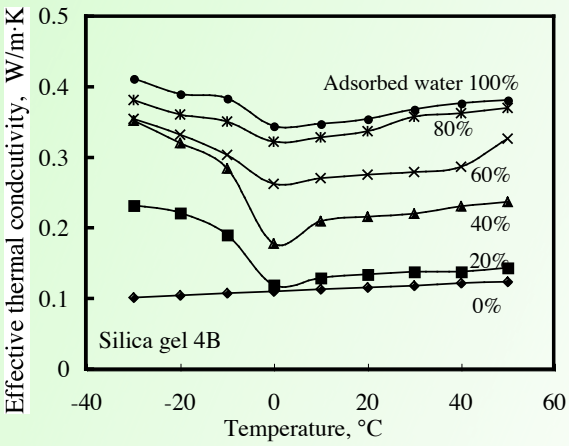

Fig.6 Effective thermal conductivity of mixture of silica gel 4B and adsorbed water

水溶液中での氷生成過程における見かけ?の熱物性

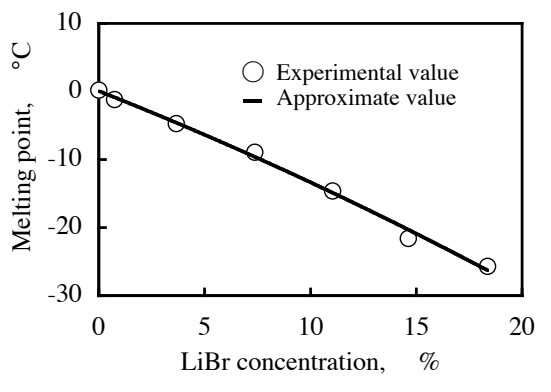

Fig.2 Relation between melting point of ice in LiBr aqueous solution and concentration

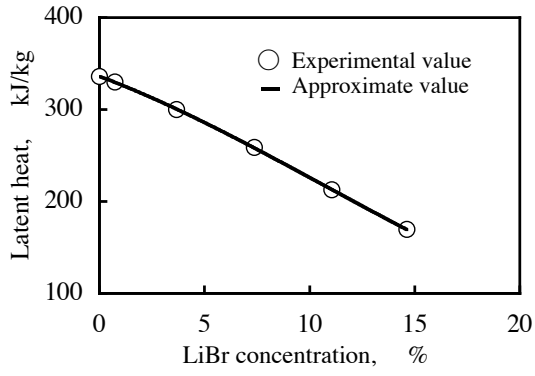

Fig.3 Relation between latent heat of ice formation in LiBr aqueous solution and concentration

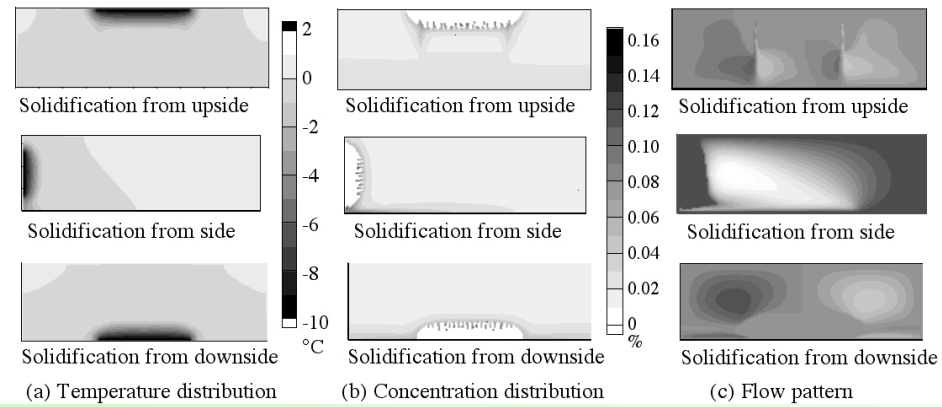

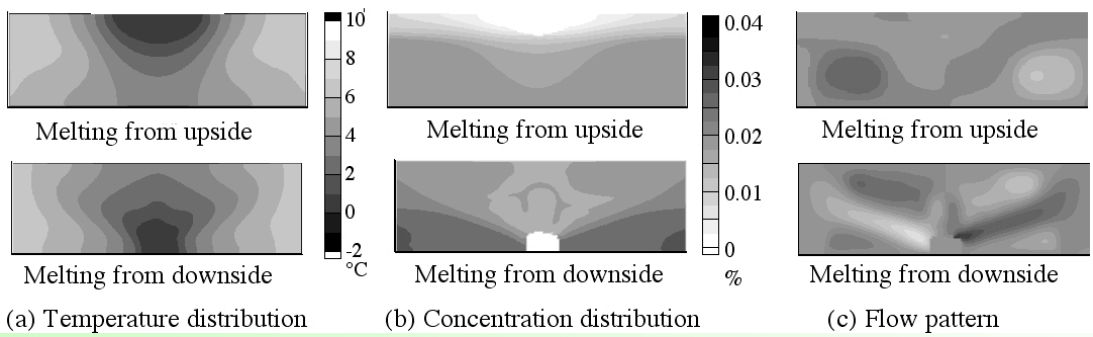

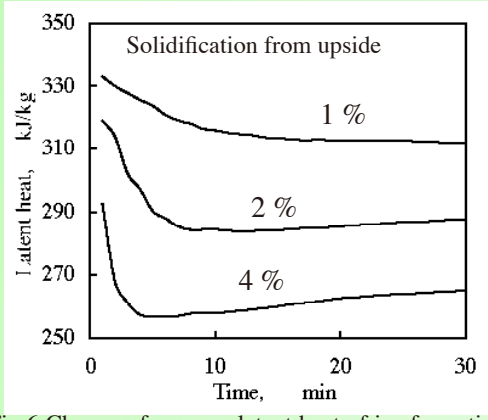

Fig.6 Change of average latent heat of ice formation in LiBr aqueous solution for various concentration

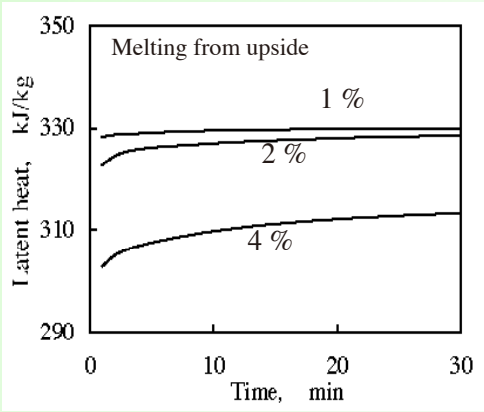

Fig.7 Change of average latent heat of ice melting in LiBr aqueous solution for various concentration

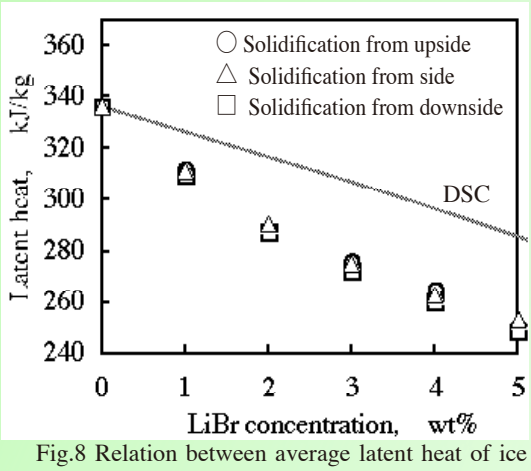

Fig.8 Relation between average latent heat of ice formation in solidification process and LiBr concentration

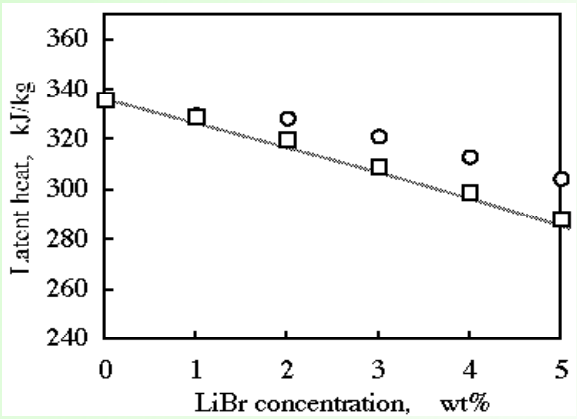

Fig.9 Relation between average latent heat of ice melting in solidification process and LiBr concentration

混合粉体の中高温域での断熱特性

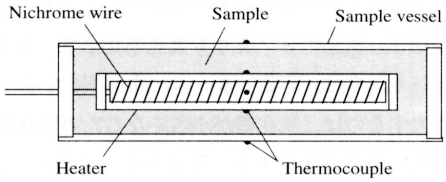

Fig. 1 Experimental apparatus for thermal conductivity measurement

Table 1 Characteristics of original sample powders

Sample	Composition	Particle size (μm)	True densitiy (kg/m^3)
Silica	SiO_2 99.9% >	0.012	2200
Titanium oxide	TiO_2 99.5% >	0.021	4200
Carbon black	C, C_mH_n etc.	0.01 ~ 0.25	1860
Fly ash	SiO_2, Al_2O_3 etc.	10 ~ 36	2210
Iron oxide	Fe_2O_3 99% >	4 ~ 5	5240

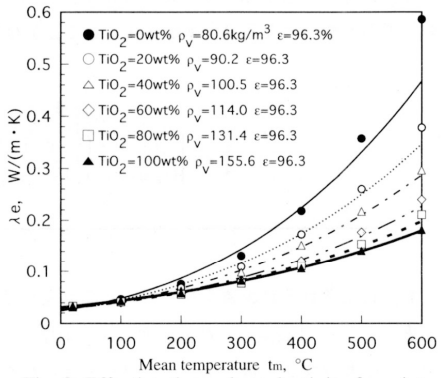

Fig. 8 Effective thermal conductivity for mixture of silica (SiO_2) and titanium oxide (TiO_2)

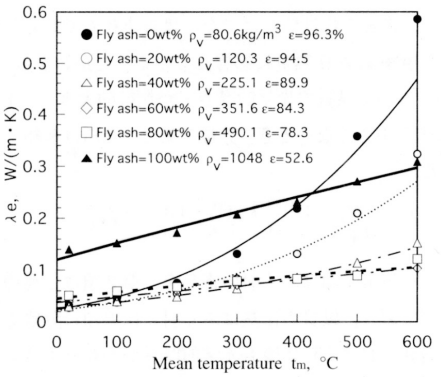

Fig. 9 Effective thermal conductivity for mixture of silica (SiO_2) and fly ash